When Helbing Meets Laumond: The Headed Social Force Model

Francesco Farina[1], Daniele Fontanelli[2], Andrea Garulli[1], Antonio Giannitrapani[1], Domenico Prattichizzo[1]

***Abstract*— The increased diffusion of service robots operating in tight collaboration with humans has renewed the interest of the scientific community towards realistic human motion models. In this paper, we present the *Headed Social Force Model*, a modeling approach enriching Helbing's Social Force Model with Laumond's human locomotion models. The proposed solution is shown to inherit the best features of either models, being able to reliably reproduce pedestrians' motions both in free space and in highly crowded environments. Extensive numerical simulations are presented in order to evaluate the performance under very different operating conditions.**

I. Introduction

Human motion models have been deeply investigated in the last decades within different research areas, ranging from building architectural design to service robotic planning and control [1]. Recently, novel applications of such models have emerged in the service robotics field. As a matter of fact, an ever growing number of applications involve robots that interact with humans for accomplishing different tasks, such as guiding visitors in a museum [2], helping navigate visually impaired people [3] or assisting older adults [4]. Guaranteeing safety is of paramount importance in human-robot interaction. In this context, accurate human motion models are required in order to predict the trajectories followed by individuals moving within the robot workspace. The same models can also be exploited for generating human-like trajectories for robots, with the purpose of increasing robot acceptance by the users (the interested reader is referred to the survey [5] for a thorough review on human-aware robot navigation).

Proposed approaches to modeling human motion include cellular automata [6], agent-based models [7] and graph-based methods [8]. One of the most popular human motion model is the *Social Force Model* (SFM), first introduced in [9] and then refined in [10] and other works by D. Helbing and his coauthors. The SFM assimilates each individual to a point-wise particle subject to social forces. In this way, the pedestrians' dynamics are described by means of a system of differential equations. The SFM is especially well suited to reproduce individual motion of pedestrians in high-density scenarios (crowd), as well as the interactions occurring among pedestrians. Recently, several experimental studies conducted by J.-P. Laumond and his research group, have revealed that in many cases the trajectories followed by pedestrians in uncluttered environments tend to comply with nonholonomic constraints [11], [12], like those featured by wheeled vehicles [13]. This phenomenon is a direct consequence of the preference of individuals towards forward motion, due to biomechanics of humans. In these circumstances, unicycle-like models are a good approximation of real-world human locomotion. For instance, unicycle kinematics is especially accurate whenever pedestrians rely on wheeled assistive aids, such as smart walkers [14]. In certain situations, however, sideward motions violating nonholonomic constraints do emerge quite naturally in practice. Avoiding an unexpected obstacle, negotiating a narrow passage or reaching a close goal are typical situations in which unicycle-like models cease to be valid. To overcome such limitations, a dynamic model that smoothly switches between holonomic and nonholonomic locomotion has been proposed in [15].

In this paper, we introduce the *Headed Social Force Model* (HSFM), an approach to modeling human locomotion which extends the traditional SFM with the inclusion of possible nonholonomic constraints. Each individual is modeled by means of a dynamic system like that presented in [15], in order to account for holonomic/nonholonomic motion patterns under different circumstances. The control inputs are designed as a suitable function of the social force acting on each individual, computed according to the traditional SFM [10]. Simulation results show that the proposed approach enjoys the best features of both Helbing's SFM and Laumond's motion models. Resulting trajectories satisfy nonholonomic constraints whenever appropriate. At the same time, the SFM ability to reproduce interactions among individuals, as well as pedestrian behavior in crowded scenarios, is preserved.

The paper is organized as follows. The two human motion models, introduced in previous works and exploited in this paper, are outlined in Section II. The Headed Social Force Model is presented in Section III. Numerical simulations highlighting some key features of the proposed approach are reported in Section IV. Finally, some conclusions are drawn in Section V.

II. Background Material

In this section, we present a brief review of the SFM presented in [10] and the human locomotion model (HLM)

This paper has received funding from the European Union's Horizon 2020 Research and Innovation Programme - Societal Challenge 1 (DG CONNECT/H) under grant agreement n° 643644 "ACANTO - A CyberphysicAl social NeTwOrk using robot friends".

[1]F. Farina, A. Garulli, A Giannitrapani and D. Prattichizzo are with the Dipartimento di Ingegneria dell'Informazione e Scienze Matematiche, Università di Siena, Siena, Italy.

[2]D. Fontanelli is with the Dipartimento di Ingegneria Industriale, Università di Trento, Trento, Italy.

proposed in [15], on which the present work relies. Vectors and matrices are written in boldface and $(\cdot)'$ denotes the transpose operator.

A. Social Force Model

Consider a system of n pedestrians moving in a 2D environment. The i-th individual, $i = 1, \dots, n$, is assimilated to a particle with mass m_i, whose position and velocity, expressed in a global reference frame, are denoted by $\mathbf{r}_i = [x_i,\ y_i]'$ and $\mathbf{v}_i = [\dot{x}_i,\ \dot{y}_i]'$, respectively. The equations of motion are then

$$\dot{\mathbf{r}}_i = \mathbf{v}_i, \tag{1}$$

$$\dot{\mathbf{v}}_i = \frac{1}{m_i}\mathbf{f}_i, \tag{2}$$

where $\mathbf{f}_i$, representing the social force driving the i-th particle, is given by the contribution of three terms

$$\mathbf{f}_i = \mathbf{f}_i^0 + \mathbf{f}_i^p + \mathbf{f}_i^w. \tag{3}$$

The first term

$$\mathbf{f}_i^0 = m_i \frac{\mathbf{v}_i^0 - \mathbf{v}_i}{\tau_i} \tag{4}$$

accounts for the pedestrian's desire to move with a given velocity vector $\mathbf{v}_i^0$. In (4), the characteristic time $\tau_i > 0$ is a parameter determining the rate of change of the velocity vector. The terms $\mathbf{f}_i^p$ and $\mathbf{f}_i^w$ represent the repulsive forces exerted on individual i by the other pedestrians and by possible obstacles present in the environment (e.g., walls), respectively. The expressions of the forces $\mathbf{f}_i^p$ and $\mathbf{f}_i^w$ are reported in the Appendix for completeness.

B. Human Locomotion Model

In the SFM, a pedestrian is modeled as a point-wise mass subject to an external force. The model does not account for the heading of the individuals (e.g., the forward direction) and, at any time, a person can move freely in any direction. However, most of the time, humans tend to move forward, i.e. their velocity vector is aligned with their heading. This phenomenon has been observed by several studies [11], [12], which come to the conclusion that a *nonholonomic* dynamic system, such as the unicycle model, could be more appropriate to describe human motion in many cases. On the other side, there are some circumstances in which sideward motions, that indeed violate the nonholonomic constraints, are commonly observed. Typical examples include navigating in highly crowded places, like exiting from a theatre, or avoiding sudden obstacles. In these cases, unicycle-like models are no longer valid and a *holonomic* model is preferable[1]. In [15], a human locomotion model (HLM) has been proposed which: i) accounts for pedestrians' heading, and ii) reproduces both holonomic and nonholonomic motion patterns by suitably controlling the system inputs. Let $\mathbf{q}_i = [\theta_i,\ \omega_i]'$ be the vector containing the heading (direction of forward locomotion) and the angular velocity of the i-th pedestrian in the global reference frame. Denote by $\mathbf{v}_i^B = [v_i^f,\ v_i^o]'$ the velocity vector expressed in body frame, i.e. in a reference frame obtained by rotating the global reference frame according to the pedestrian's heading θ_i. The components v_i^f and v_i^o of vector $\mathbf{v}_i^B$ correspond to the projection of the velocity vector along the forward direction and the orthogonal direction, respectively. Clearly, $\mathbf{v}_i = \mathbf{R}(\theta_i)\mathbf{v}_i^B$, where the rotation matrix $\mathbf{R}(\theta_i)$ is defined as

$$\mathbf{R}(\theta_i) = \begin{bmatrix} \cos(\theta_i) & -\sin(\theta_i) \\ \sin(\theta_i) & \cos(\theta_i) \end{bmatrix}.$$

Then, the HLM can be written as

$$\dot{\mathbf{r}}_i = \mathbf{R}(\theta_i)\mathbf{v}_i^B, \tag{5}$$

$$\dot{\mathbf{v}}_i^B = \frac{1}{m_i}\mathbf{u}_i^B, \tag{6}$$

$$\dot{\mathbf{q}}_i = \mathbf{A}\mathbf{q}_i + \mathbf{b}_i u_i^\theta, \tag{7}$$

where

$$\mathbf{A} = \begin{bmatrix} 0 & 1 \\ 0 & 0 \end{bmatrix}, \quad \mathbf{b}_i = \begin{bmatrix} 0 \\ \frac{1}{I_i} \end{bmatrix}, \tag{8}$$

and I_i denotes the moment of inertia of pedestrian i. In the HLM, the control inputs are $\mathbf{u}_i^B = [u_i^f,\ u_i^o]'$, whose entries are the forces acting along the forward direction and the sideward direction, respectively, as well as the torque u_i^θ about the vertical axis. Notice that the model (5)-(7) is indeed a holonomic model. However, if $v_i^o(0) = 0$ and $u_i^o(t) = 0$, for all t, the HLM boils down to the dynamic unicycle model. In general, whenever $v_i^o = 0$, the HLM features a nonholonomic behavior, the velocity vector being aligned with the pedestrian's heading.

Remark 1: In [15], a single pedestrian is considered and the HLM is instrumental to formulating and solving an inverse optimal control problem aimed at identifying optimality criteria guiding human motion. In this paper, we are interested in modeling the motion of multiple individuals, as well as the interactions occurring among them, and between people and environment. To this purpose, the approach followed in this work is to enrich the traditional SFM with an enhanced model of human motion model like the HLM.

III. Headed Social Force Model

The scheme of the Headed Social Force Model proposed in this work is shown in Fig. 1. The basic idea is to exploit the SFM to evaluate at each time instant the social forces $\mathbf{f}_i$ and $\mathbf{f}_i^0$ acting on a pedestrian according to (3)-(4), and then computing the HLM control inputs $\mathbf{u}_i^B$ and u_i^θ as suitable functions of $\mathbf{f}_i$ and $\mathbf{f}_i^0$, as described below.

A. Control Input $\mathbf{u}_i^B$

The input vector $\mathbf{u}_i^B$ includes the forces acting along the pedestrian's forward direction (identified by the heading θ_i) and the sideward direction (i.e., orthogonal to the heading θ_i). Given the total social force $\mathbf{f}_i$, a natural choice for computing u_i^f and u_i^o is to project $\mathbf{f}_i$ along the forward and sideward directions, respectively. This is done by rotating $\mathbf{f}_i$ according to the matrix $\mathbf{R}(\theta_i)'$. In order to avoid sideward motions if

[1]With a slight abuse of terminology, we denote by "holonomic model" a model not subject to nonholonomic constraints, thus including unconstrained models.

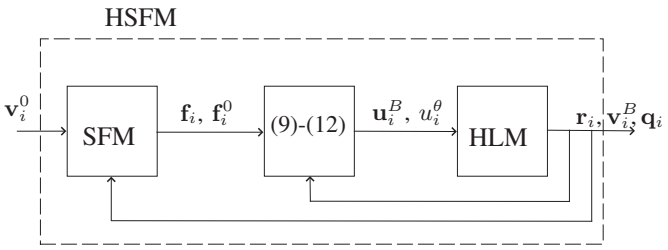

Fig. 1. Block diagram of the Headed Social Force Model.

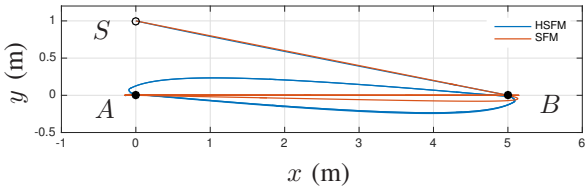

Fig. 2. Scenario I. A single pedestrian has to move back and forth between A and B, starting from an arbitrary initial position S, with a desired speed $v^0 = 1.5$ ms^{-1}: SFM (red) and HSFM (blue).

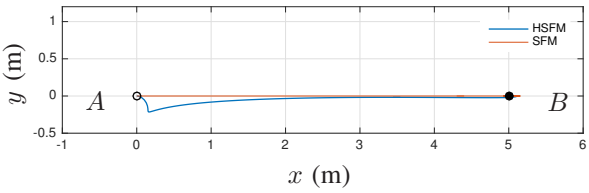

Fig. 3. Scenario I. A single pedestrian has to move from A to B, starting with the point B behind her back, with a desired speed $v^0 = 1.5$ ms^{-1}: SFM (red) and HSFM (blue).

not strictly needed, i.e. in order to reproduce a nonholonomic behavior as much as possible, the components u_i^f and u_i^o can be weighted differently, the weight assigned to u_i^o being smaller than that assigned to u_i^f. Finally, in order to drive to zero the sideward velocity v_i^o when the sideward force is zero, a damping term proportional to $-v_i^o$ can be added to u_i^o. Hence, the control input $\mathbf{u}_i^B$ is computed as

$$\mathbf{u}_i^B = \mathbf{K}^B \mathbf{R}(\theta_i)' \mathbf{f}_i - \mathbf{k}^d v_i^o, \tag{9}$$

where

$$\mathbf{K}^B = \begin{bmatrix} k^f & 0 \\ 0 & k^o \end{bmatrix}, \quad \mathbf{k}^d = \begin{bmatrix} 0 \\ k^d \end{bmatrix},$$

and k^f, k^o, and k^d are positive constant parameters. Notice that if $k^f = k^o = 1$, $k^d = 0$ and the pedestrian's heading is constant, i.e. $\dot{\theta}_i = 0$ for all t, then the dynamic model (5)-(6), with $\mathbf{u}_i^B$ given by (9), boils down to the traditional SFM (1)-(2). However, if θ_i varies with time, the trajectories generated by (5)-(6) with input (9) are in general different from those resulting from (1)-(2).

B. Control Input u_i^θ

The input u_i^θ represents the torque about the vertical axis which drives the dynamics of the pedestrian's heading. This term is designed on the basis of the force $\mathbf{f}_i^0$ defined in (4). Recall that such a term accounts for the individual's intent of moving according to a desired velocity vector $\mathbf{v}_i^0$. In a sense, $\mathbf{f}_i^0$ models long-term objectives, such as passing through a given sequence of way-points, whereas the forces $\mathbf{f}_i^p$ and $\mathbf{f}_i^w$ accounts for short-term corrective actions, such as maneuvers needed to avoid nearby obstacles or pedestrians. Denote by f_i^0 and θ_i^0 the magnitude and the phase in the global reference frame of the force term $\mathbf{f}_i^0$. Notice that both quantities are in general time-varying. The input u_i^θ is computed as

$$u_i^\theta = -k^\theta(\theta_i - \theta_i^0) - k^\omega \omega_i. \tag{10}$$

The parameters k^θ and k^ω are designed in order to achieve a suitable dynamic performance. It can be easily verified that, with u_i^θ defined as in (10), the orientation error $\tilde{\theta}_i \doteq \theta_i - \theta_i^0$ evolves according to the dynamic model

$$\ddot{\tilde{\theta}}_i + \frac{k^\omega}{I_i}\dot{\tilde{\theta}}_i + \frac{k^\theta}{I_i}\tilde{\theta}_i = -\frac{k^\omega}{I_i}\dot{\theta}_i^0 - \ddot{\theta}_i^0. \tag{11}$$

A possible design procedure is to select the values of k^θ and k^ω on the basis of the desired poles λ_1 and λ_2 of the dynamic system (11). In this work, desired real poles are considered, so that $\lambda_2 = \alpha\lambda_1 < 0$, for some $\alpha > 1$. In turn, the dominant pole λ_1 is selected as a function of f_i^0

$$\lambda_1 = -\sqrt{\frac{k^\lambda f_i^0}{\alpha}},$$

where $k^\lambda > 0$ is a constant parameter. The corresponding expressions of k^θ and k^ω are then

$$k^\theta = I_i k^\lambda f_i^0, \quad k^\omega = I_i(1+\alpha)\sqrt{\frac{k^\lambda f_i^0}{\alpha}}. \tag{12}$$

The choice of time-varying poles allows one to modulate the responsiveness of the system with the intensity of the driving force $\mathbf{f}_i^0$. The underlying idea is that the more authoritative the $\mathbf{f}_i^0$, the faster the change in the pedestrian's heading. In this way, the heading convergence rate is proportional to f_i^0.

IV. Numerical Results

In this section, numerical simulations are presented to demonstrate how, using the HSFM, each agent smoothly switches between holonomic and nonholonomic behaviors, depending on the current external conditions. The value of the parameters of the SFM are taken from [10] and are reported in the Appendix. The reference velocity vector $\mathbf{v}_i^0$ in (4) is generated as $\mathbf{v}_i^0 = v^0 \mathbf{e}_i^0$. The desired speed v^0 is assumed constant in all the simulations. The unit vector $\mathbf{e}_i^0$, which identifies the desired direction of motion, is computed from a sequence of way-points encoding the desired pedestrian path, similarly to [9]. The inertia moment I_i in (8) is computed from the pedestrian's mass m_i and radius r_i as $I_i = \frac{1}{2} m_i r_i^2$. The following parameters of the control law (9)-(12) have been used in all the simulations: $k_f = 1$, $k^o = 0.3$, $k_d = 5$, $\alpha = 3$ and $k^\lambda = 0.02$. Three different scenarios

are simulated, each of them highlighting a characteristic feature of the proposed model. Videos of some simulations are available at http://control.dii.unisi.it/MobileRoboticsPage.

A. Scenario I: The Nonholonomic Behavior

Empirical evidence shows that when a single pedestrian is moving in an open space, she tends to move as a unicycle [12]. In this respect, a good model is expected to be able to reproduce such a nonholonomic behavior.

Let us consider a simple example, in which a single pedestrian walks between two points A and B, alternately, starting from an arbitrary point S. In this case, the trajectory resulting from the SFM is quite unnatural. Once point A is reached for the first time, the trajectory boils down to a segment (see red line in Fig. 2). This phenomenon is due to the SFM neglecting the information about the pedestrian's heading, so that forward or backward motions become equivalent. On the contrary, the trajectory generated by the HSFM is more realistic thanks to the existence of a preferred direction of motion (see blue line in Fig. 2). Although the HSFM allows a pedestrian to have her velocity vector not aligned with her heading, the control input $\mathbf{u}_i^B$ tends to drive the orthogonal component of the velocity to zero if no lateral forces are present ("almost nonholonomic" behavior).

In the same scenario, consider the case in which a pedestrian has to move from A to B, starting with the initial heading $\theta_i(0) = \pi$, i.e. the goal point B is behind pedestrian's back. As shown in Fig. 3, using the HSFM, the pedestrian takes a step back to turn towards the goal, and then moves forward to reach the target. Clearly, the SFM trajectory lies on a segment once again, since the heading is neglected.

The previous examples confirm that, in the considered scenario, the HSFM yields a more realistic behavior, giving to the pedestrian the ability of moving in a nonholonomic way when she is expected to do so.

B. Scenario II: The Adaptive Behavior

While human motion tends to be fully nonholonomic in open spaces, a holonomic behavior is typically observed in crowded environments. This second set of simulations aim at showing the HSFM ability of adapting to external conditions by automatically switching between the two behaviors. In Scenario II, a group of 20 pedestrians, walking in the same direction in a 7m-wide corridor at a desired speed $v^0 = 1.5$ ms^{-1}, have to pass through a 2m-wide door. In Fig. 4, a snapshot of a simulation run, taken while pedestrians are crossing the door, is depicted. The adaptive behavior of the HSFM can be inferred by looking at Fig. 5, where the ratio $\frac{v_i^o}{v_i^f}$ is shown for all the pedestrians. Such a quantity is a measure of the misalignment between the velocity vector and the pedestrian's heading, being zero in correspondence of a nonholonomic motion. It can be seen that, after a transient during which all the pedestrians align their velocity vector towards the desired direction of motion, the ratio $\frac{v_i^o}{v_i^f}$ is always almost zero, except during the door crossing. This means that, in the corridor, where the pedestrians' density is relatively low, the resulting trajectories do not differ much from those of a traditional unicycle. On the contrary, during the door crossing, significant sideward motions are taken by the pedestrians in order to avoid contacts. It is worth stressing that this qualitatively different beahviors are automatically reproduced by a single instance of the HSFM, without the need of modifying the value of any of its parameters.

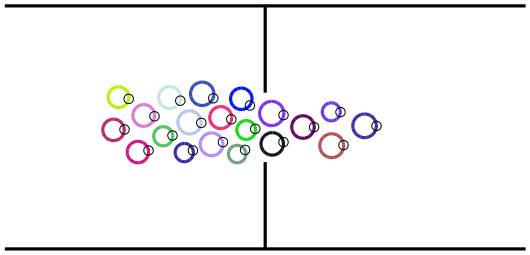

Fig. 4. Scenario II. A group of 20 pedestrians walking in the same direction in a 7m-wide corridor at a desired speed $v^0 = 1.5$ ms^{-1}. A snapshot of a simulation run of the HSFM, taken while pedestrians are crossing the door.

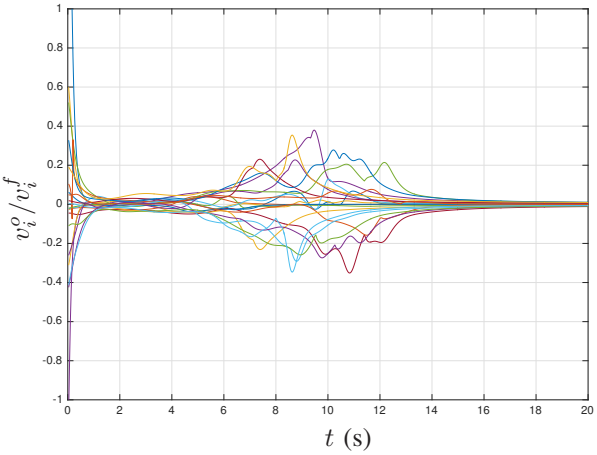

Fig. 5. Scenario II. Ratio $\frac{v_i^o}{v_i^f}$ for $i = 1, \ldots, 20$.

In order to compare the trajectories generated by the SFM and the HSFM, a Monte Carlo analysis has been performed. Starting from random initial positions and headings of the pedestrians (with zero initial velocity), 100 runs of the SFM and the HSFM have been simulated for 20 s. For comparison purposes, the following indicators have been considered:

- the average *exit frequency* of pedestrians $\overline{F}$, i.e. the average number of pedestrians that pass through the door per unit time;

- the average *bending energy* of the trajectories

$$\overline{B} = \frac{1}{n}\sum_{i=1}^{n}\frac{1}{T}\int_0^T \kappa_i(t)^2 dt, \tag{13}$$

where the curvature $\kappa_i(t)$ of the i-th trajectory is defined as

$$\kappa_i = \frac{\dot{x}_i\ddot{y}_i - \ddot{x}_i\dot{y}_i}{(\dot{x}_i^2 + \dot{y}_i^2)^{\frac{3}{2}}}; \tag{14}$$

- the average *squared magnitude of the jerk* of the trajectories

$$\overline{J} = \frac{1}{n}\sum_{i=1}^{n}\frac{1}{T}\int_0^T ||\mathbf{j}_i(t)||^2 dt, \tag{15}$$

where $\mathbf{j}_i = \ddot{\mathbf{v}}_i$ is the jerk vector of the i-th trajectory.

The first indicator has been selected as a measure of the macroscopic behavior of the models. The last two indicators are used to evaluate the regularity of the resulting trajectories. The bending energy is a measure of the smoothness of a trajectory [16], whereas the jerk is commonly used in transportation systems to evaluate the user's comfort associated to a given trajectory.

Concerning the exit frequency, both models give similar results, with average values $\overline{F}_{HSFM} = 2.73$ s^{-1} and $\overline{F}_{SFM} = 2.77$ s^{-1}. Also the empirical distributions of the exit frequency, computed from the trajectories generated by the SFM and the HSFM, are very similar. Overall the two models seem to reproduce the same macroscopic behavior. However, significant differences can be appreciated by looking at the regularity of the resulting trajectories. The average bending energy is $\overline{B}_{HSFM} = 85$ m^{-2} and $\overline{B}_{SFM} = 1.440$ m^{-2}, for the HSFM and the SFM, respectively. Also the squared magnitude of the jerk is very different in the two cases, with average values $\overline{J}_{HSFM} = 2.14 \cdot 10^{-5}$ m^{2}s^{-6} and $\overline{J}_{SFM} = 1.57 \cdot 10^{-4}$ m^{2}s^{-6}. These figures capture the different qualitative behaviors that can be observed by looking at the resulting trajectories. When compared to the HSFM, in the proximity of the door, the SFM tends to generate vibrations, sudden changes of direction and even "bounces" among pedestrians or between pedestrians and walls. To get an idea of the very different motion patterns resulting from the two models, in Fig. 6 the magnitude of the jerk and the curvature as a function of time, during a single run, are reported for all the pedestrians.

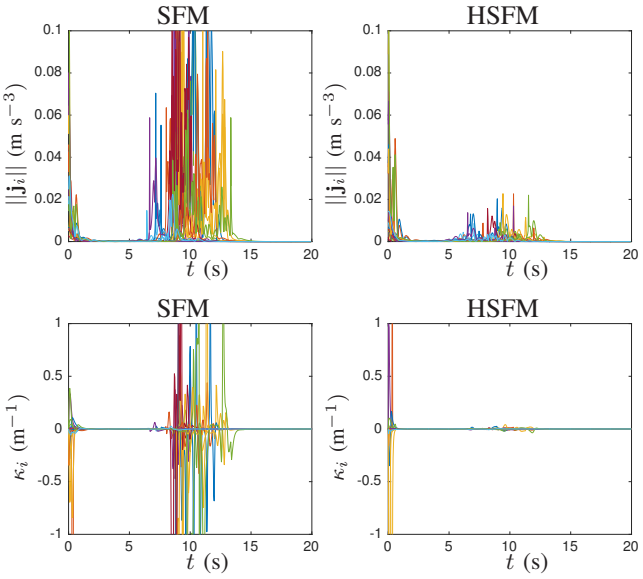

Fig. 6. Scenario II. Magnitude of the jerk (first row) and curvature (second row) for the trajectories generated by the SFM (first column) and the HSFM (second column).

C. Scenario III: A Highly Crowded Environment

The objective of simulations carried out in the third scenario is to evaluate to what extent the HSFM is able to preserve the good predictive capability of the SFM in the presence of a high density of pedestrians. As a matter of fact, the SFM is very accurate when modeling highly crowded environment, such as escape panic situations.

To this aim, we have simulated the same evacuation example presented in [10], in which 200 pedestrians must evacuate a 15m×15m room through a door of width 1 m. In these conditions, the exit becomes a bottleneck and arching and clogging arise in the proximity of the door. In [10], it was studied how the exit frequency varies with the desired speed v^0 of the pedestrians. As expected, at slow speeds, the frequency grows with v^0. However, when v^0 exceeds a threshold value (about 1.5 ms^{-1}) the frequency drops due to the increased jam induced by panic (the so called "faster-is-slower" effect). In order to evaluate the ability of the HSFM to reproduce such a phenomenon, the evacuation experiment has been simulated for 60 s, at different desired speeds, ranging from 0.5 ms^{-1} to 6 ms^{-1}. For each simulation run, the average exit frequency resulting from the SFM and the HSFM has been computed. The results are pretty similar (see Fig. 7), thus confirming the adequateness of the HSFM also in highly crowded environments.

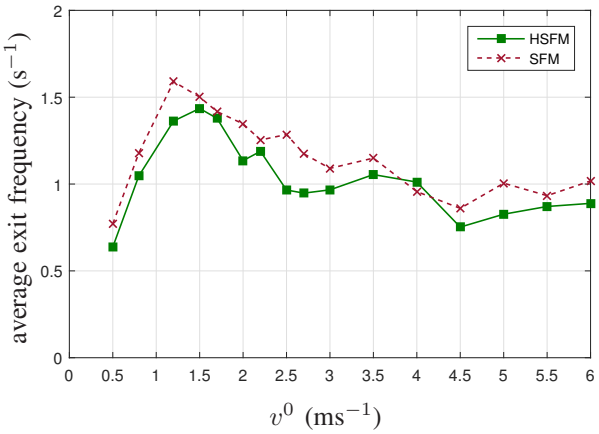

Fig. 7. Scenario III. Average exit frequency: SFM (dashed red) and HSFM (solid green).

V. Conclusions

In this paper, a new human motion model, called Headed Social Force Model, has been proposed. It combines together the pros of the traditional Social Force Model with a more realistic dynamic model of human locomotion. It is shown that the HSFM is able to reproduce both nonholonomic motion patterns (like those typically followed by pedestrians moving in free spaces) and holonomic behaviors, such as sideward motions that naturally arise in crowded environments. One key feature of the proposed model is its ability to automatically adapt the characteristics of the generated trajectory to the external conditions, without the need of changing the values of the model parameters or even switching between different models.

This work is still in a preliminary stage and a number of developments are currently under investigation. Among them, the most important one is the enhancement of the model with the inclusion of additional force terms to reproduce the typical behavior of people moving in group.

Appendix

A. Repulsive Forces in the SFM

The complete expressions of $\mathbf{f}_i^p$ and $\mathbf{f}_i^w$ in (3) are reported hereafter. Let the radius of the i-th pedestrian be denoted by r_i. Moreover, let us define

$$r_{ij} = r_i + r_j, \tag{16}$$

$$d_{ij} = \|\mathbf{r}_i - \mathbf{r}_j\|, \tag{17}$$

$$\mathbf{n}_{ij} = \frac{\mathbf{r}_i - \mathbf{r}_j}{\|\mathbf{r}_i - \mathbf{r}_j\|} \doteq [\mathbf{n}_{ij}(1),\ \mathbf{n}_{ij}(2)]', \tag{18}$$

$$\mathbf{t}_{ij} = [-\mathbf{n}_{ij}(2),\ \mathbf{n}_{ij}(1)]', \tag{19}$$

$$\Delta v_{ij}^{(t)} = (\mathbf{v}_j - \mathbf{v}_i)'\mathbf{t}_{ij}. \tag{20}$$

- The term $\mathbf{f}_i^p$, modeling the repulsive effects of other pedestrians on individual i, is given by $\mathbf{f}_i^p = \sum_{j,\ j\neq i} \mathbf{f}_{ij}^p$. The force exerted by pedestrian j on pedestrian i is

$$\mathbf{f}_{ij}^p = \left[A_i e^{(r_{ij}-d_{ij})/B_i} + k_1 g(r_{ij} - d_{ij})\right] \mathbf{n}_{ij} + k_2 g(r_{ij} - d_{ij}) \Delta v_{ij}^{(t)} \mathbf{t}_{ij}, \tag{21}$$

  where $g(x) = \max\{0,\ x\}$ and A_i, B_i, k_1 and k_2 are constant parameters. Notice how $\mathbf{f}_{ij}$ is composed by three terms. The first one, $A_i e^{(r_{ij}-d_{ij})/B_i}\mathbf{n}_{ij}$, represents the repulsive term, while $k_1 g(r_{ij} - d_{ij})\mathbf{n}_{ij}$ and $k_2 g(r_{ij} - d_{ij})\Delta v_{ij}^{(t)}\mathbf{t}_{ij}$ represent the compression and friction forces, respectively, and come into play only if $d_{ij} < r_{ij}$.
- The term $\mathbf{f}_i^w$, modeling the repulsive effects of obstacles or boundaries such as walls on individual i, is given by $\mathbf{f}_i^w = \sum_w \mathbf{f}_{iw}^w$. The force exerted by wall w on pedestrian i is

$$\mathbf{f}_{iw}^w = \left[A_w e^{(r_i-d_{iw})/B_w} + k_1 g(r_i - d_{iw})\right] \mathbf{n}_{iw} - k_2 g(r_i - d_{iw}) \Delta v_{iw}^{(t)} \mathbf{t}_{iw}. \tag{22}$$

  The expression of $\mathbf{f}_{iw}^w$ is is pretty similar to that of the repulsive force between pedestrians $\mathbf{f}_{ij}^p$. Quantities d_{iw}, $\mathbf{n}_{iw}$, $\mathbf{t}_{iw}$ and $\Delta v_{iw}^{(t)}$ are defined according to (17)-(20), by replacing $\mathbf{r}_j$ with the coordinates of the closest point of wall w to pedestrian i and setting $\mathbf{v}_j = 0$.

In this paper, the radius r_i and the mass m_i of each pedestrian have been randomly generated in the intervals $[0.25\text{ m},\ 0.35\text{ m}]$ and $[60\text{ kg},\ 90\text{ kg}]$, respectively, assuming uniform distributions. In accordance with [10], the following parameters have been used for all i and w: $\tau_i = 0.5\,\text{s}$, $A_i = A_w = 2 \cdot 10^3\,\text{N}$, $B_i = B_w = 0.08\,\text{m}$, $k_1 = 1.2 \cdot 10^5\,\text{kg}\,\text{s}^{-2}$, $k_2 = 2.4 \cdot 10^5\,\text{kg}\,\text{m}^{-1}\text{s}^{-1}$.

References

[1] X. Zheng, T. Zhong, and M. Liu, "Modeling crowd evacuation of a building based on seven methodological approaches," *Building and Environment*, vol. 44, no. 3, pp. 437–445, 2009.

[2] S. Thrun, M. Beetz, M. Bennewitz, W. Burgard, A. B. Cremers, F. Dellaert, D. Fox, D. Haehnel, C. Rosenberg, N. Roy *et al.*, "Probabilistic algorithms and the interactive museum tour-guide robot minerva," *The International Journal of Robotics Research*, vol. 19, no. 11, pp. 972–999, 2000.

[3] V. Kulyukin, C. Gharpure, J. Nicholson, and G. Osborne, "Robot-assisted wayfinding for the visually impaired in structured indoor environments," *Autonomous Robots*, vol. 21, no. 1, pp. 29–41, 2006.

[4] L. Palopoli, A. Argyros, J. Birchbauer, A. Colombo, D. Fontanelli, A. Legay, A. Garulli, A. Giannitrapani, D. Macii, F. Moro, P. Nazemzadeh, P. Padeleris, R. Passerone, G. Poier, D. Prattichizzo, T. Rizano, L. Rizzon, S. Scheggi, and S. Sedwards, "Navigation assistance and guidance of older adults across complex public spaces: the DALi approach," *Intelligent Service Robotics*, vol. 8, no. 2, pp. 77–92, 2015.

[5] T. Kruse, A. K. Pandey, R. Alami, and A. Kirsch, "Human-aware robot navigation: A survey," *Robotics and Autonomous Systems*, vol. 61, no. 12, pp. 1726–1743, 2013.

[6] C. Burstedde, K. Klauck, A. Schadschneider, and J. Zittartz, "Simulation of pedestrian dynamics using a two-dimensional cellular automaton," *Physica A: Statistical Mechanics and its Applications*, vol. 295, no. 3-4, pp. 507 – 525, 2001.

[7] Q. Zhu, "Hidden Markov model for dynamic obstacle avoidance of mobile robot navigation," *IEEE Transactions on Robotics and Automation*, vol. 7, no. 3, pp. 390–397, Jun 1991.

[8] M. Bennewitz, W. Burgard, G. Cielniak, and S. Thrun, "Learning motion patterns of people for compliant robot motion," *The International Journal of Robotics Research*, vol. 24, no. 1, pp. 31–48, 2005.

[9] D. Helbing and P. Molnár, "Social force model for pedestrian dynamics," *Phys. Rev. E*, vol. 51, pp. 4282–4286, 1995.

[10] D. Helbing, I. Farkas, and T. Vicsek, "Simulating dynamical features of escape panic," *Nature*, vol. 407, pp. 487–490, September 2000.

[11] G. Arechavaleta, J.-P. Laumond, H. Hicheur, and A. Berthoz, "An optimality principle governing human walking," *IEEE Transactions on Robotics*, vol. 24, no. 1, pp. 5–14, 2008.

[12] ——, "On the nonholonomic nature of human locomotion," *Autonomous Robots*, vol. 25, no. 1-2, pp. 25–35, 2008.

[13] G. Ferrer and A. Sanfeliu, "Proactive kinodynamic planning using the extended social force model and human motion prediction in urban environments," in *2014 IEEE/RSJ International Conference on Intelligent Robots and Systems*. IEEE, 2014, pp. 1730–1735.

[14] D. Fontanelli, A. Giannitrapani, L. Palopoli, and D. Prattichizzo, "A passive guidance system for a robotic walking assistant using brakes," in *Proceedings of the 54th IEEE Conference on Decision and Control*, Osaka (JP), Dec 15-18 2015, pp. 829–834.

[15] K. Mombaur, A. Truong, and J.-P. Laumond, "From human to humanoid locomotion – an inverse optimal control approach," *Autonomous robots*, vol. 28, no. 3, pp. 369–383, 2010.

[16] F. Dayoub, G. Cielniak, and T. Duckett, "Eight weeks of episodic visual navigation inside a non-stationary environment using adaptive spherical views," in *Field and Service Robotics*, 2015, pp. 379–392.